

Investigating the shadows of new regular black holes with a Minkowski core: Effects of spherical accretion and core type differences

Yi Xiong^{1,*}, Jin Pu^{1,†}, Yi Ling^{2,3,‡}, Guo-Ping Li^{1,§} and Gao-Ming Deng¹

¹*School of Physics and Astronomy, China West Normal University, Nanchong 637002, China*

²*Institute of High Energy Physics, Chinese Academy of Sciences, Beijing 100049, China*

³*School of Physics, University of Chinese Academy of Sciences, Beijing 100049, China*

We investigate the shadows and optical appearances of a new type of regular black holes (BHs) with a Minkowski core under different spherical accretion. These BHs are constructed by modifying the Newtonian potential based on the minimum observable length in the Generalized Uncertainty Principle (GUP). They correspond one-to-one with the traditional regular BHs with a de-Sitter (dS) core (such as Bardeen/Hayward BHs), characterized by quantum gravity effect parameter (α_0) and spacetime deformation factor (n). We find that the characteristic parameters give rise to some novel observable features. For these new BHs, the shadow radius, photon sphere radius, and total observed intensity increase with the increase of α_0 but decrease with the increase of n . Under different spherical accretion, the shadow and photon sphere radius are identical, but the total observed intensity under the static spherical accretion is greater than that under the infalling spherical accretion. In addition, we find that these regular BHs with different cores show differences in shadows and optical appearances, especially under the static spherical accretion. Compared with Bardeen BH, the new BH has a smaller total observed intensity, dimmer maximum luminosity, and smaller shadow and photon sphere radius. The larger α_0 leads to more significant differences, and a similar trend is also seen in the comparison with Hayward BH. Under the infalling spherical accretion, these regular BHs with different cores only have slight differences in total observed intensity, shadow and photon sphere radius, which become more obvious when α_0 is relatively large. It suggests that the unique spacetime features of these regular BHs with different cores can be distinguished through astronomical observations.

*email: 960318449@qq.com

†email: pujin@cwnu.edu.cn

‡email: lingy@ihep.ac.cn

§email: gpliphys@yeah.net

I. Introduction

The prediction of BHs by General Relativity (GR) has always been a hot topic of scientific research, sparking widespread attention and academic debate. After the Laser Interferometer Gravitational-Wave Observatory (LIGO) first detected gravitational waves from the merger of binary BHs [1, 2], LIGO and its partners have recorded nearly a hundred such binary events. These observations not only validate GR but also provide rich data for BH research. Later, the Event Horizon Telescope (EHT) collaboration published the first ultra-high angular resolution image of the supermassive BH in the Messier 87 (M87*) galaxy, marking a significant milestone in astrophysical research [3]. The image revealed a bright ring-like structure surrounding the central dark region, known as the BH shadow, which is formed by light being strongly bent and focused as it approaches the BH's edge. This ring-like structure is referred to as the photon ring. The strong gravitational field around the BH is a crucial factor in the formation of the shadow. Furthermore, EHT's polarization measurements have revealed the significant impact of the strong magnetic field at the edge of the BH on the behavior of surrounding matter, confirming that the magnetic field structure around the M87* BH's accretion disk aligns with the predictions of general relativistic magnetohydrodynamics (GRMHD) models [4]. These findings contribute to our understanding of the physical processes around BHs, including the infall of matter into BHs and the formation of BH jets. Afterwards, EHT captured the first hierarchical radio observation image of the Sagittarius A* (SgrA*) BH at the center of our Milky Way galaxy, which is mainly composed of a bright thick ring [5]. These observations suggest that the accretion disk may influence the observational characteristics of the BH shadows, offering a new perspective for studying BH shadows.

Indeed, the theoretical analysis of the shadow formation of Schwarzschild BH was proposed even before EHT [6]. Here, the escaping cone of photon was defined by the impact parameter corresponding to the critical curve, which is known as the BH shadow. Later, Bardeen examined the D-shaped shadow of the Kerr BH, which arises from the dragging effect of the rotating BH on the path of light rays [7]. Additionally, the actual astrophysical BHs in the universe are always encircled by various accretion materials, which are of paramount importance for the observation and imaging of BHs. Consequently, Shakura and Sunyaev postulated a standard thin accretion disk model, assuming the accretion disks are geometrically thin, optically thick, and in a steady state [8]. This model predicts the disk's geometric configuration, optical properties, and spectral characteristics, providing a theoretical foundation for understanding the fundamental nature and energy release of accretion disks. This model is also in alignment with numerous BH observational

phenomena. Using this thin accretion disk model, Luminet simulated the first image of a BH with an emitting accretion disk using a semi-analytic method, visually illustrating the gravitational lensing effect and the formation of the photon ring [9]. However, to more closely approximate the accretion flows around BHs in the realistic astrophysical environment, it is necessary to consider the interaction of magnetic fields, which requires numerical simulations using GRMHD to extract the BH images. It is worth noting that in most cases, in order to reveal the basic characteristics of BH images and the behavior of strong gravitational fields, using some toy models of accretion structures is sufficient for research. In this sense, Wald et al. studied the radiation from optically and geometrically thin disk accretion around Schwarzschild BHs, categorizing it into direct, lensed ring, and photon ring emissions [10]. They found that the observed BH images are primarily dominated by the direct emissions, with smaller contributions from lensed ring emissions and negligible contributions from photon ring emissions. The observed appearance of the BH shadow depends on the emission details and morphology of the disk accretion, including the geometry of the emission region, the emission profile, and the optical depth. This initiated a series of research efforts on various toy accretion models for different types of BHs [11–21]. Spherical accretion, as a simplified toy accretion model, has also garnered widespread attention [22–28]. In this model, the size and shape of the BH shadow are mainly determined by the spacetime geometry of the BH, rather than the specific details of the accretion process. Thus, a large number of simulations of various BH shadows have been widely discussed, as shown in examples and references therein [29–46]. These studies indicate that the properties of BH shadows are closely related to the spacetime background, which also provides a potential method for distinguishing BHs in GR from other alternative compact objects or BHs in alternative theories beyond GR.

On the other hand, to avoid the infamous singularity problem, researchers have proposed constructing some regular BHs without singularity phenomenologically by introducing some exotic matter that violates standard energy conditions or through quantum corrections to spacetime geometry [47–57]. Traditional regular BHs, such as Bardeen/Hayward/Frolov BHs, have a dS core at their centers. Recently, a new type of regular BHs with sub-Planckian curvature was introduced in [58, 59], which is characterized by an exponentially suppressed Newtonian potential and an asymptotically Minkowski core. These new regular BHs can reproduce the metric of Bardeen/Hayward/Frolov BHs on large scales by choosing different forms of the potential, and is derived from GUP in curved spacetime. Such regular BHs with a Minkowski core have also been reported in [60, 61], but our understanding of them remains incomplete. Hence, exploring the connection between these new regular BHs and astronomical observations to search for any signs

or traits that might indicate that the BHs observed in the cosmos belong to the regular type rather than the traditional singular BHs, has become an intriguing endeavor.

Evidently, at this juncture, it is impractical to differentiate between singular BHs and regular BHs by diving into the event horizon or detecting any signals from their interiors. Nevertheless, the distinctions within the BHs might manifest in external phenomena, such as the photon sphere or the trajectories of massive particles [62–74]. Therefore, in [62], we meticulously examined the photon spheres and marginally stable circular orbits for regular BHs with two distinct cores: these new regular BHs with a Minkowski core, and Bardeen/Hayward BHs with a dS core. The results show that the positions of the photon sphere and the marginally stable circular orbits for the compact massive object (CMO) phase with a Minkowski core are notably distinct from their counterparts in the CMO phase with a dS core. Following this, in [15], we investigated the thin accretion disks of regular BHs with a Minkowski core that can reproduce Bardeen BH at large scales, and compared them with the accretion disks around Bardeen BH with a dS core. The results reveal that the thin accretion disks of these regular BHs with different cores exhibit distinct astronomical optical characteristics.

On this basis, we will extend the work presented in [15] by studying images of these new regular BHs with a Minkowski core under the spherical accretion, and comparing them with those of traditional regular BHs with a dS core. This provides the theoretical foundation for distinguishing between the two types of regular BHs with different cores through astronomical observations. More importantly, in [62], we found that for the regular BHs with a Minkowski core, different choices of the potential form result in different positions of the photon spheres and marginally stable circular orbits in the CMO phase. Additionally, it was observed in [15] that the optical characteristics of Bardeen and Hayward BHs, surrounded by thin accretion disks, exhibit distinct differences. In particular, the Hayward BH exhibits a minimal distance between the innermost region of the direct image and the outermost region of the secondary image, which is anticipated to serve as an identifier for distinguishing the Hayward BH. These findings have sparked our interest in exploring whether there are also distinct differences in the images of these new regular BHs with a Minkowski core under the spherical accretion model, which would be a very meaningful pursuit.

The paper is organized as follows. In Sec.II, we briefly review these new regular BHs with a Minkowski core, which can reproduce the characteristics of traditional regular BHs on large scales, and compare the behavior of light rays around these regular BHs with different cores by using a ray tracing code. In Sec.III, we will study the shadow and optical appearances of these new regular BHs with a Minkowski core under two types of spherical accretion. In Sec.IV, we will

compare the shadows of the regular BHs with a Minkowski core with those of traditional regular BHs (Bardeen/Hayward BHs) with a dS core. Our conclusions and discussions are presented in Sec.V.

II. The new regular BHs with a Minkowski core

In order to avoid singularity, the key to constructing the regular BH at the phenomenological level is to obtain a finite value for Kretschmann scalar curvature. A new type of regular BHs with an asymptotically Minkowski core was proposed in [58]. The metric for this type of regular BHs is given by

$$ds^2 = -\left(1 + 2\psi(r)\right)dt^2 + \frac{1}{1 + 2\psi(r)}dr^2 + r^2d\Omega^2, \quad (1)$$

where the gravitation potential $\psi(r)$ is defined as

$$\psi(r) = -\frac{M}{r}e^{-\alpha_0\frac{M^x}{r^n}}. \quad (2)$$

The dimensionless parameter α_0 is induced by quantum gravity effect. The gravitation potential has an exponentially suppressed form, and the motivation stems from the modification of the standard Heisenberg uncertainty principle due to quantum gravity [75–80].

The dimensionless parameters x and n together determine the behavior of Kretschmann scalar curvature at the core, where they must satisfy the conditions $n \geq x \geq n/3$ and $n \geq 2$ in order to ensure the existence of the event horizon and maintain the scalar curvature at sub-Planckian levels. Obviously, as r approaches 0, the spacetime is dominated by a Minkowski core. Moreover, for certain values of x and n , a one-to-one correspondence can be established between such new regular BHs with a Minkowski core and those with a dS core on large scales [58]. Specifically, for the new regular BHs that have a Minkowski core, as outlined in Eq.(2), there exists the corresponding traditional regular BHs with a dS core, and their gravitation potentials are given by

$$\psi(r) = -\frac{Mr^{\frac{n}{x}-1}}{(r^n + x\alpha_0M^x)^{1/x}}. \quad (3)$$

Observe that on large scales, the new regular BH with parameters $x = 2/3$ and $n = 2$ corresponds to Bardeen BH, while with parameters $x = 1$ and $n = 3$, it corresponds to Hayward BH. This indicates that the two types of regular BHs exhibit the same asymptotic behavior on large scales, but they have distinct cores at their centers. It should be noted that for these new regular BHs with a Minkowski core, the quantum gravity effect parameter α_0 must be within the range $0 \leq \alpha_0 \leq 0.73M$

for the case of $x = 2/3$ and $n = 2$, and within the range $0 \leq \alpha_0 \leq 0.98M$ for $x = 1$ and $n = 3$ to ensure the existence of the horizon. When $\alpha_0 = 0$, it returns to the standard Schwarzschild BH. The horizon of the line element given in Eq.(1) is determined by solving $1 + 2\psi(r_h) = 0$.

Next we examine the motion of photons near these new regular BHs. The motion of these photons is governed by the Euler-Lagrange equation, which is expressed as follows

$$\frac{d}{d\lambda} \left(\frac{\partial \mathcal{L}}{\partial \dot{x}^\mu} \right) = \frac{\partial \mathcal{L}}{\partial x^\mu}. \quad (4)$$

Here, λ is an affine parameter, and \dot{x}^μ represents the four-velocity of the photon. In the context of a static spacetime, the Lagrangian density \mathcal{L} is expressed as

$$\mathcal{L} = -\frac{1}{2} g_{\mu\nu} \frac{dx^\mu}{d\lambda} \frac{dx^\nu}{d\lambda} = -\frac{1}{2} \left[-f(r)\dot{t}^2 + f^{-1}(r)\dot{r}^2 + r^2 \left(\dot{\theta}^2 + \sin^2 \theta \dot{\phi}^2 \right) \right]. \quad (5)$$

For photons, the Lagrangian density $\mathcal{L} = 0$. In a spherically symmetric spacetime, we analyze the motion of photons restricted to the equatorial plane of these new regular BHs by setting $\theta = \pi/2$ and $\dot{\theta} = 0$. Since the Lagrangian density is zero and the metric coefficients cannot be explicitly solved in terms of the t and θ coordinates, there exist two conserved quantities, E and L , representing the energy and angular momentum of the photons respectively

$$E = f(r) \left(\frac{dt}{d\lambda} \right), \quad L = r^2 \left(\frac{d\phi}{d\lambda} \right). \quad (6)$$

The four-velocity is given by

$$\frac{dt}{d\lambda} = \frac{1}{bf(r)}, \quad \frac{d\phi}{d\lambda} = \pm \frac{1}{r^2}, \quad \frac{dr}{d\lambda} = \sqrt{\frac{1}{b^2} - \frac{f(r)}{r^2}}. \quad (7)$$

Here, the \pm signs denote the direction of photon motion on the equatorial plane: the “+” sign corresponds to clockwise motion, and the “-” sign corresponds to counterclockwise motion. The impact parameter b is defined as

$$b = \frac{|L|}{E} = \frac{r^2 \dot{\phi}}{f(r)\dot{t}}, \quad (8)$$

and the effective potential $V_{\text{eff}}(r)$ is given by

$$V_{\text{eff}}(r) = \frac{1}{r^2} \left(1 + 2\psi(r) \right). \quad (9)$$

For null geodesics, where $g_{\mu\nu} \dot{x}^\mu \dot{x}^\nu = 0$, we can obtain the first-order differential equation of motion

$$\dot{r}^2 + V_{\text{eff}} = \frac{1}{b^2}. \quad (10)$$

Obviously, for photons to form a photon sphere, their circular orbit must satisfy $\dot{r} = 0$ and $\ddot{r} = 0$. Mathematically, this means

$$V'_{\text{eff}}(r_c) = 0, \quad V_{\text{eff}}(r_c) = \frac{1}{b_c^2}. \quad (11)$$

Here, r_c represents the radius of the photon sphere, and b_c denotes the corresponding critical impact parameter, which is related to the shadow radius of these new regular BHs.

Parameter	Type	r_h	r_c	b_c
$\alpha_0 = 0$	Schwarzschild	2.00000	3.00000	5.19615
$\alpha_0 = 0.3$	$x = 2/3, n = 2$	1.82833	2.81574	5.00833
	Bardeen	1.83402	2.81929	5.01087
$\alpha_0 = 0.72$	$x = 2/3, n = 2$	1.33657	2.44678	4.66393
	Bardeen	1.49244	2.48965	4.69073

The locations of the event horizon (r_h), the photon sphere (r_c), and the critical impact parameter (b_c) of the new regular black hole ($x = 2/3, n = 2$) and the Bardeen black hole for various values of α_0 . We set $M = 1$.

Parameter	Type	r_h	r_c	b_c
$\alpha_0 = 0.3$	$x = 1, n = 3$	1.91656	2.9290	5.13562
	Hayward	1.91849	2.92968	5.13600
$\alpha_0 = 0.72$	$x = 1, n = 3$	1.74762	2.80996	5.03894
	Hayward	1.77024	2.81540	5.04179
$\alpha_0 = 0.92$	$x = 1, n = 3$	1.59272	2.74067	4.98595
	Hayward	1.67020	2.75161	4.99145

The locations of the event horizon, the photon sphere, and the critical impact parameter of the new regular BH ($x = 1, n = 3$) and the Hayward BH with the various α_0 . We set $M = 1$.

We present in Table I and II the numerical results for the event horizon r_h , the photon sphere r_c , and the critical impact parameter b_c corresponding to various values of the parameter α_0 . The results indicate that the values of r_h , r_c , and b_c of Schwarzschild BH are greater than those of these new regular BHs. As the parameter α_0 increases, the values of r_h , r_c , and b_c of these new regular

BHs decrease. For a given α_0 , the values of r_h , r_c , and b_c of these new regular BHs are related to the spacetime deformation parameters (x and n) and the type of core they possess. When the core type is the same, these values increase with the increase of the dimensionless parameters (x and n). This means that for the new regular BH, when $x = 1$ and $n = 3$, their values are greater than those when $x = 2/3$ and $n = 2$, and the values of Hayward BH are greater than those of Bardeen BH. When the dimensionless parameters (x and n) are the same, the traditional regular BHs with a dS core are slightly greater values than these new regular BHs with a Minkowski core, and this discrepancy becomes more significant as the parameter α_0 increases. This means that Bardeen BH with a dS core is slightly greater values than the one with a Minkowski core ($x = 2/3$ and $n = 2$), and similarly, Hayward BH with a dS core is slightly greater values than the one with a Minkowski core ($x = 2/3$ and $n = 2$).

Later, in order to better understand how the specific parameters affect the photon trajectories and their classification, we describe the motion of photons around these new regular BHs by tracking the change in the radial coordinate as a function of the azimuthal angle ϕ . By introducing the parameter $u = 1/r$, we are able to derive the trajectory equation

$$\frac{du}{d\phi} = \sqrt{\frac{1}{b^2} - u^2 (1 - 2Mue^{-\alpha_0 M u^n})}. \quad (12)$$

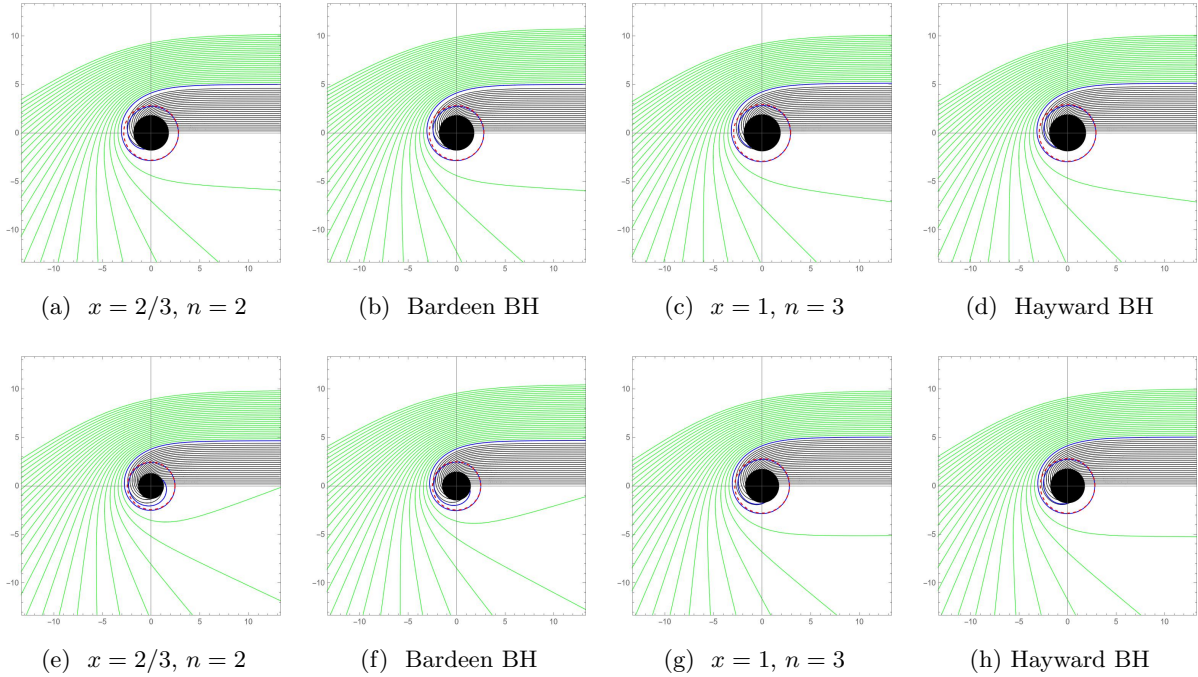
and the azimuthal angle ϕ can be integrated out as

$$\phi = \int \frac{1}{\sqrt{b^{-2} - u^2 (1 - 2Mue^{-\alpha_0 M u^n})}} du \quad (13)$$

Based on the above formulas, we numerically simulated the turning points of photon trajectories around these new regular BHs and analyzed the corresponding geodesic geometry. To accurately distinguish among different light trajectories, we used polar coordinates (b, ϕ) and employed a ray tracing code to plot the paths of light as it moves around these new regular BHs, as shown in Fig.1. These plots demonstrate the changes in trajectories for different impact parameters b , with the distance between the different impact parameters b being 0.2.

In Fig.1, the black disk represents the boundary of the event horizon, and the red dashed circle denotes the trajectory of light rays with the critical parameter $b = b_c$ which finally forms the photon sphere. For $b < b_c$, the light trajectories are engulfed by these regular BHs, making them invisible to an observer at infinity, as shown by the black lines in Fig.1. For $b > b_c$, the light trajectories are deflected, enabling them to reach an observer at infinity, as shown by the green lines in Fig.1. Moreover, as the parameter α_0 increases, the area in which the light trajectories are captured by these regular BHs decreases, as shown in Table I and II. Additionally, the area in which the light

trajectories are captured by these regular BHs is also related to the dimensionless parameters (x and n) and the type of core they possess, as shown in Table I and II. Fig.1 shows that for the same core, the area of the new regular BH with the parameters $x = 1$ and $n = 3$ is greater than that with $x = 2/3$ and $n = 2$, and Hayward BH has a greater area than Bardeen BH. For the same dimensionless parameters (x and n), the area of Bardeen BH with a dS core is slightly greater than that with a Minkowski core ($x = 2/3$ and $n = 2$), and the area of Hayward BH with a dS core is slightly greater than that with a Minkowski core ($x = 2/3$ and $n = 2$).



The trajectories of light rays for the regular BHs with different cores. The top and bottom plots correspond to $\alpha_0 = 0.3$ and $\alpha_0 = 0.72$, respectively. We set $M = 1$.

These results indicate that the changes in the parameters induced by quantum gravity effect (represented by α_0) and spacetime deformation (characterized by x and n) can modify the size of these shadows and their ability to capture photons. In particular, as the parameter α_0 increases, the differences in the motion of photons around these new regular BHs with different parameters (x and n) and distinct cores become more evident. This finding offer crucial clues for further research on the impact of quantum gravity and spacetime structure on the images of these new regular BHs under the spherical accretion models in the next section.

III. Images of the new regular BHs with a Minkowski core

In this section, we will investigate the shadow images of these new regular BHs with a Minkowski core, considering two models of spherically symmetric accretion: static spherical accretion and infalling spherical accretion. We will examine the impact of the parameter (α_0) that is induced by quantum gravity effects and the parameter (n) that describes the formation of various spacetime structures on the observational characteristics of the shadow.

A. Static spherical accretion

Generally, when matter in the universe is captured by a BH, the morphology of the accretion flow around the BH is governed by its angular momentum. High angular momentum causes the matter to form a disk-like accretion, whereas with extremely low angular momentum, the matter flows radially towards the BH, leading to a spherically symmetric accretion [80–86]. We first investigate the shadow images and photon spheres of these new regular BHs with a Minkowski core surrounded by the static spherical accretion. This assumes that the accretion is static relative to these new regular BHs. For an observer at infinity, the observed specific intensity $I(\nu_o)$ (measured in $\text{erg s}^{-1} \text{cm}^{-2} \text{str}^{-1} \text{Hz}^{-1}$) is determined by integrating the specific emissivity along the photon path γ [85, 86], i.e.

$$I(\nu_o) = \int_{\gamma} g^3 j_e(\nu_e) dl_{prop}. \quad (14)$$

Here, ν_o is the frequency of the observed photon, and ν_e is the frequency of the emitted photon. The redshift factor g is defined as $g = \nu_o/\nu_e = f(r)^{1/2}$. In the rest frame of the emitter, $j_e(\nu_e)$ represents the emissivity per unit volume and is typically given by the form $j_e(\nu_e) \propto \delta(\nu_r - \nu_e)/r^2$, where ν_r is the frequency in the emitter's rest frame [86]. The infinitesimal proper length dl_{prop} is given by

$$dl_{prop} = \sqrt{\frac{1}{f(r)} dr^2 + r^2 d\phi^2} = \sqrt{\frac{1}{f(r)} + r^2 \left(\frac{d\phi}{dr}\right)^2} dr, \quad (15)$$

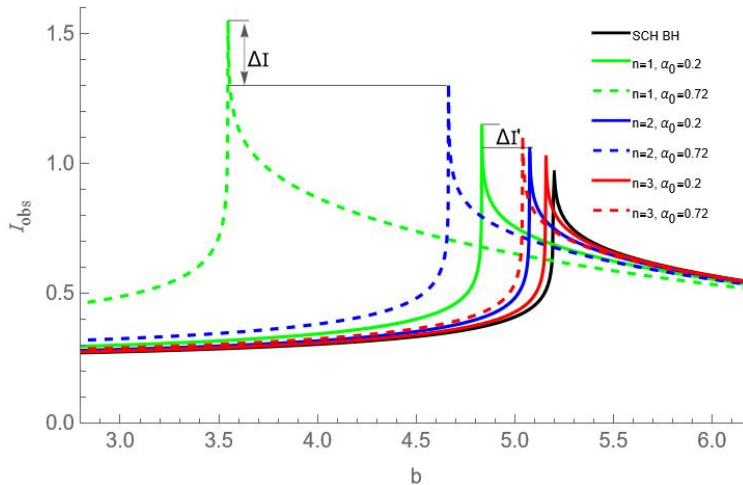
where $d\phi/dr$ is obtained by Eq.(12). Subsequently, integrating Eq.(14) over all observed frequencies gives the total observed intensity, expressed as

$$I_{obs} = \int_{\nu_o} I(\nu_o) d\nu_o = \int_{\nu_e} \int_{\gamma} g^4 j_e(\nu_e) dl_{prop} d\nu_e = \int_{\gamma} \frac{f(r)^2}{r^2} \sqrt{\frac{1}{f(r)} + r^2 \left(\frac{d\phi}{dr}\right)^2} dr. \quad (16)$$

According to Eq.(16), we can investigate the shadow images and the total observed intensities of these new regular BHs with a Minkowski core surrounded by the static spherical accretion model.

It is noteworthy that we aim to study how variations in the quantum gravity effect parameter (α_0) and spacetime deformation (n) affect the total observed intensities.

We compared the cases with $x = 2/3$ and $n = 2$ to those with $x = 1$ and $n = 3$. In Fig.2, we illustrate the trend of the total observed intensities at spatial infinity as a function of the impact parameter b . It is evident that the total observed intensity increases gradually with b when $b < b_c$, but it rises sharply as it approaches b_c , reaching a maximum at this position. Following this, as the value of b continues to increase beyond b_c , the total observed intensity begins to decrease gradually, eventually approaching zero at infinity.



The variation of the total observed intensities radiated from the static spherical accretion with the impact parameter under different values of α_0 and n . We set $M = 1$.

Fig.2 shows that the peak value of total observed intensity for these new regular BHs with a Minkowski core is consistently higher than that of Schwarzschild BH. When the spacetime deformation $n = 1$, the maximum observed intensity for the new regular BH corresponding to $\alpha_0 = 0.72$ (shown as the green dashed line) is greater than the case with $\alpha_0 = 0.2$ (shown as the green solid line). Similarly, for the spacetime deformation factors $n = 2$ and $n = 3$, the maximum observed intensities corresponding to $\alpha_0 = 0.72$ (shown as the blue and red dashed lines) are also greater than those for $\alpha_0 = 0.2$ (shown as the blue and red solid lines). These results imply that the larger the value of α_0 , the stronger the total observed intensity of these new regular BHs. Notably, the parameter α_0 arises from the corrections due to quantum gravity effect, indicating that the stronger the quantum gravity effect, the higher the luminosity of these new regular BHs, thereby enabling the observer to capture more luminous information.

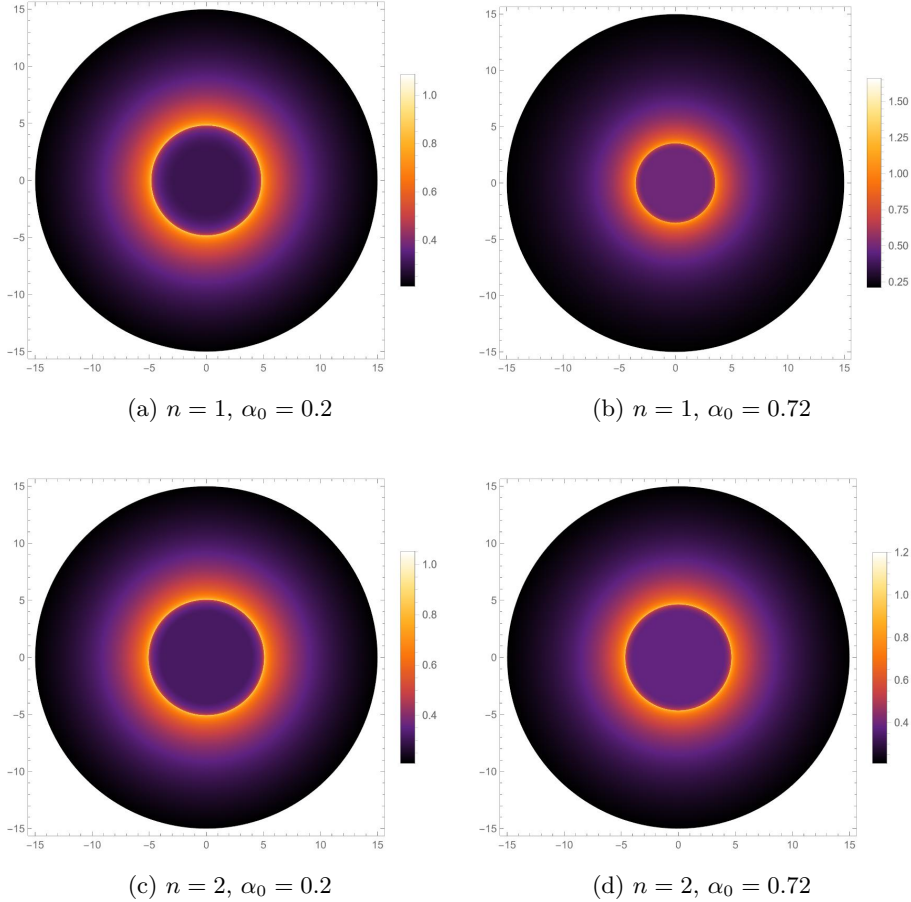
Furthermore, Fig.2 illustrates that for the parameter $\alpha_0 = 0.72$, the maximum value of the

total observed intensity decreases in the order of $n = 1$, $n = 2$, and $n = 3$, corresponding to the green dashed line, blue dashed line, and red dashed line, respectively. Similarly, for the parameter $\alpha_0 = 0.2$, the maximum value of the observed intensity also decreases sequentially for $n = 1$, $n = 2$, and $n = 3$, corresponding to the green solid line, blue solid line, and red solid line, respectively. This implies that as the parameter n increases, the total observed intensity of these new regular BHs gradually weakens, indicating that a smaller value of n can increase the optical brightness and enable the observer to detect more luminous signals.

Finally, in Fig.2, ΔI represents the difference in the maximum value of the total observed intensities for $n = 1$ and $n = 2$ corresponding to $\alpha_0 = 0.72$, and $\Delta I'$ represents the difference $n = 1$ and $n = 2$ corresponding to $\alpha_0 = 0.2$. It is evident that ΔI is greater than $\Delta I'$, which means that the difference between the maximum intensities becomes more pronounced as the parameter α_0 increases. This indicates that the larger α_0 , the easier it is to distinguish between these new regular BHs with different n through the total observed intensity. We take $n = 1$ and $n = 2$ as examples and present the two-dimensional image of the total observed intensity for these new regular BHs with different α_0 in Fig.3.

In Fig.3, the photon sphere is at the bright ring with the strongest luminosity. It can be observed that the inner region of the photon sphere is not completely dark, as a small fraction of the radiation can escape from these new regular BHs, so a weak luminosity can be observed near the photon sphere. Obviously, the parameters α_0 and n have a significant impact on both the maximum luminosity and the faint illuminating region in the shadow images of these new regular BHs. By comparing Fig.(3a) with Fig.(3b) and (3c) with Fig.(3d), we can see that for a given n , the larger α_0 leads to a brighter maximum light intensity of the BH image, but a smaller radius of the BH shadow and photon sphere. By comparing Fig.(3c) with Fig.(3d) and Fig.(3b) with Fig.(3d), we can see that for a given α_0 , the larger n leads to a darker maximum light intensity of the BH image, but a larger radius of the BH shadow and photon sphere.

In addition, the contrast between the observed intensity and the radius of the faint illuminating region is greater in Figs.3b and 3d than in Figs.(3a) and (3c). It indicates that as α_0 increases, the differences between the shadow images for $n = 1$ and $n = 2$ become more apparent. Therefore, under the static spherical accretion model, the enhancement of quantum gravity effect can increase the luminosity of photon ring and enlarge the shadow size for these new regular BHs. As n decreases, the enhancement of quantum gravity effect becomes more pronounced. This is because a smaller n amplifies the influence of α_0 on the optical characteristics of these new regular BHs, thereby making it easier for the observer to distinguish these new regular BHs.



The optical appearances of these new regular BHs under the static spherical accretion for different values of α_0 and n .

B. Infalling spherical accretion

In this section, we will investigate the shadow images of these new regular BHs with a Minkowski core surrounded by an infalling spherical accretion. This is a dynamical model where the accretion is assumed to move radially towards the BH. In this case, the observed specific intensity in Eq.(14) is still applicable, but the corresponding redshift factor differs from the one in static spherical accretion. The redshift factor in the infalling spherical accretion can be expressed as

$$g_i = \frac{\mathcal{K}_\rho u_0^\rho}{\mathcal{K}_\sigma u_e^\sigma}, \quad \mathcal{K}^\mu = \dot{x}_\mu \quad (17)$$

Here, \mathcal{K}_μ represents the four-velocity of a photon emitted by the accreting matter. $u_0^\rho = (1, 0, 0, 0)$ corresponds to the four-velocity of a static observer, and u_e^σ denotes the four-velocity of the infalling

accretion, given by

$$u_e^t = \frac{1}{f(r)}, \quad u_e^r = -\sqrt{1-f(r)}, \quad u_e^\theta = u_e^\phi = 0. \quad (18)$$

The four-velocity of the photon is derived from the null geodesic, which is

$$K_t = \frac{1}{b}, \quad K_r = \pm \frac{1}{f(r)} \sqrt{\frac{1}{b^2} - \frac{f(r)}{r^2}}. \quad (19)$$

It is noted that in k_r , the + or - sign indicates whether the photon is moving radially inward or outward from the BH. For the case of the infalling spherical accretion, the redshift factor can be written as

$$g_i = \left[u_e^t + \left(\frac{K_r}{K_t} \right) u_e^r \right]^{-1}. \quad (20)$$

Furthermore, unlike the static spherical accretion case, the proper distance is expressed as

$$dl_{\text{prop}} = K_\mu u_e^\mu d\lambda = \frac{K_t}{g_i |K_r|} dr. \quad (21)$$

The total observed intensity for the infalling spherical accretion is calculated as follows

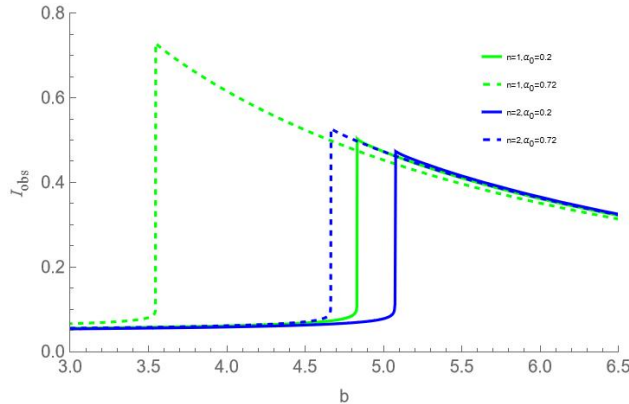
$$I_{\text{obs}} = \int_\gamma \frac{g_i^3 K_t}{r^2 |K_r|} dr. \quad (22)$$

Based on the above equation, we obtain the variation of the total observed intensity I_{obs} with the impact parameter b under different parameters α_0 and n , observed by an observer at infinity.

We select the cases of $\alpha_0 = 0.2$ and $\alpha_0 = 0.72$, and $n = 1$ and $n = 2$ to draw Fig.4. It can be found that as the impact parameter b increases, the total observed intensity increases slowly. When the impact parameter b approaches the critical value b_c , the total observed intensity increases rapidly and reaches a peak. Subsequently, as b continues to increase, the total observed intensity gradually decreases. At the same time, the variation of the total observed intensity is closely related to the parameters n and α_0 . For a fixed n , with the increase of α_0 , the impact parameters b corresponding to the peak position of the total observed intensity decreases, and the total observed intensity corresponding to the peak increases. For a fixed α_0 , with the increase of n , the impact parameters b corresponding to the peak position of the total observed intensity increases, and the peak value of the total observed intensity decreases.

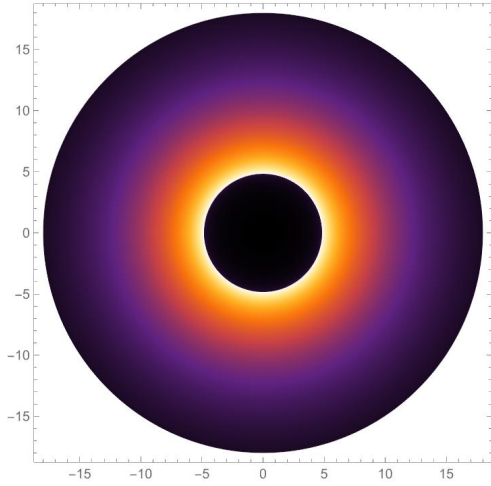
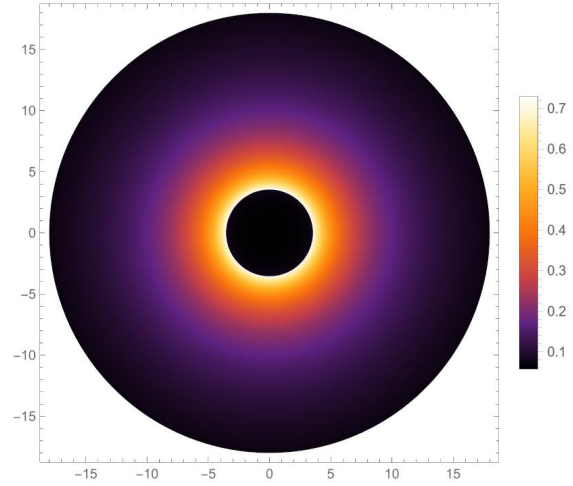
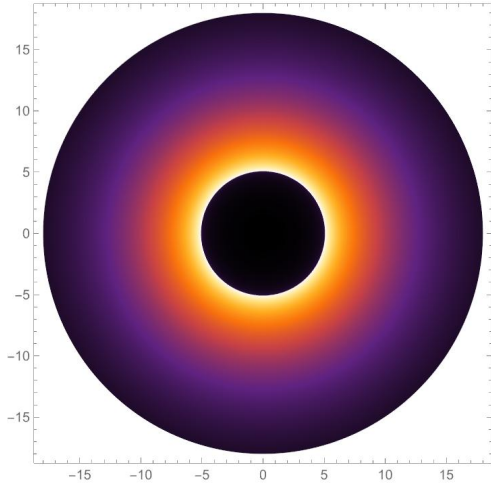
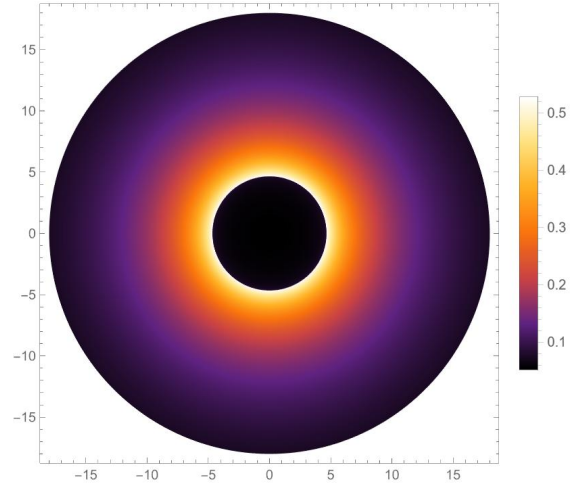
Fig.5 shows the optical appearances of these new regular BHs under the infalling spherical accretion. By comparing Figs.(5a) and (5b), it can be found that as α_0 increases, the maximum luminosity of the total observed intensity becomes larger, while the radius of the shadow and the photon sphere become smaller. Conversely, by comparing Figs.(5c) and (5d), as the parameter

n increases, the maximum luminosity of the total observed intensity becomes smaller, and the radius of the shadow and the photon sphere become larger. At the same time, by comparing the differences in the maximum luminosity and the shadow radius between Figs.(5a) and (5c), as well as between Figs.(5b) and (5d), it can be found that as the parameter α_0 increases, the differences in the optical appearances of $n = 1$ and $n = 2$ become more obvious. Therefore, under the infalling spherical accretion, the larger α_0 is, the greater the luminosity of the photon ring and the larger the shadow size are. Conversely, as the parameter n increases, the luminosity of the photon ring and the shadow size decrease.



The variation of the total observed intensities radiated from the infalling spherical accretion with the impact parameter under different values of α_0 and n . We set $M = 1$.

Combining the results in Fig.3 under the static spherical accretion and those in Fig.5 under the infalling spherical accretion, for an observer at infinity, the total observed intensity, the shadow radius, and the photon sphere radius of these new regular BHs with a Minkowski core are closely related to the intrinsic parameters of the BH themselves. Under both spherical accretion, the larger α_0 is, the larger the total observed intensity, the shadow radius, and the photon sphere radius of these new regular BHs will be. Conversely, the larger n is, the smaller these values will be. Then, by comparing the results of the two spherical accretion, it is found that the size of the shadow radius and the photon sphere radius of these new regular BHs is independent of the choice of the spherical accretion model. However, the total observed intensity of these new regular BHs is related to the choice of the spherical accretion model. The total observed intensity obtained from the static spherical accretion is much larger than that from the infalling spherical accretion. This indicates that the BH shadow can represent the intrinsic properties of the BH spacetime, and the choice of the accretion model only affects the total observed intensity of the shadow, not the structure of the BH shadow itself. Therefore, the spacetime characteristics of these new regular

(a) $n = 1, \alpha_0 = 0.2$ (b) $n = 1, \alpha_0 = 0.72$ (c) $n = 2, \alpha_0 = 0.2$ (d) $n = 2, \alpha_0 = 0.72$

The optical appearances of these new regular BHs under the infalling spherical accretion for different values of α_0 and n .

BHs can be distinguished by observing and studying the BH shadow.

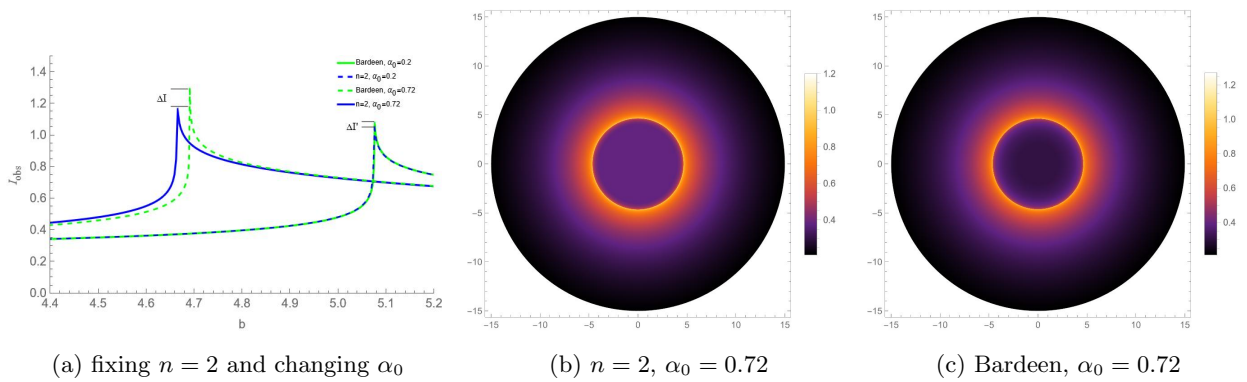
In the next section, we will further compare the shadows formed by these new regular BHs with a Minkowski core and the traditional regular BHs with a dS core under the two different spherical accretion, and discuss the application of shadow research in distinguishing regular BHs with different cores.

IV. Comparison with the traditional regular BHs

As previously mentioned, these new regular BHs exhibit similar asymptotic behavior to the traditional Bardeen/Hayward BHs on large scales, but they differ in the core of the central region. Specifically, these new regular BHs have a Minkowski core, while the traditional Bardeen/Hayward BHs have a dS core. It has been found that in the thin disk accretion model of [15], the optical observational characteristics of the new regular BH and the corresponding traditional Bardeen BH may differ. Based on this, in this section, we will further compare the shadows and optical appearances of these new regular BHs with those of the corresponding traditional Bardeen/Hayward BHs under the spherical accretion model. Meanwhile, the research in the previous section shows that different spherical accretion models can affect the total observed intensities of the shadows. Therefore, we will also compare the shadows of these new regular BHs and the corresponding traditional regular BHs under two different spherical accretion models.

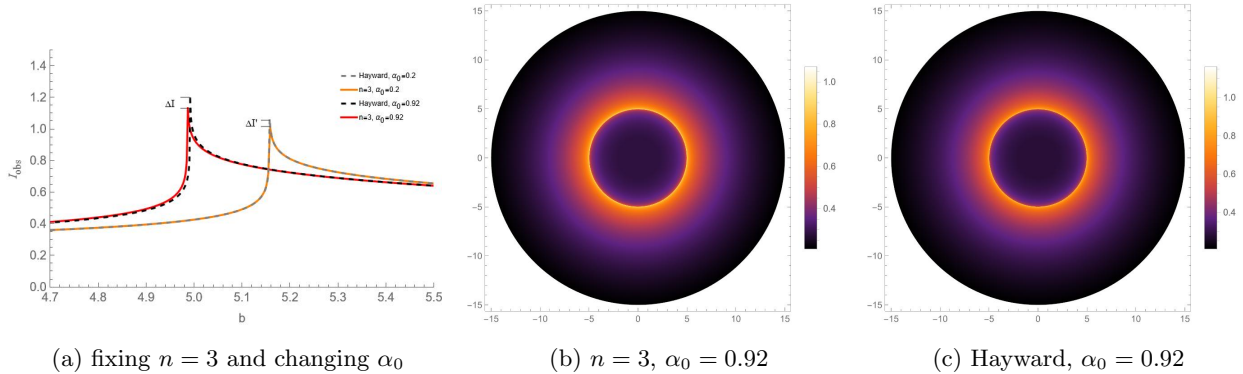
A. Comparison under the static spherical accretion

According to the previous discussion, when $n = 2$, $x = 2/3$, and when $n = 3$, $x = 1$, these new regular BHs show a one-to-one correspondence with the Bardeen BH and the Hayward BH respectively on a large scale. It is noted that the cores of these new regular BHs and the traditional regular BHs are different at the center. To compare the shadows of regular BHs with different cores, Figs.6 and 7 present the total observed intensities and optical appearances of the two types of regular BHs with different cores under the static accretion.



The total observed intensities and the optical appearances under the static spherical accretion for the new regular BH with $n = 2$ and the corresponding Bardeen BH.

Firstly, from Figs.(6a) and (7a), it can be observed that the peak value of the total observed intensity of these new regular BHs with a Minkowski core is always smaller than that of the traditional regular BHs with a dS core. Here, ΔI and $\Delta I'$ represent the differences in the peak values of the total observed intensities of these regular BHs with different cores at the same α_0 respectively, and $\Delta I > \Delta I'$. This implies that the larger α_0 is, the more obvious the difference in the peak values of these BHs with different cores becomes, and the more significant the corresponding difference in the total observed intensity is.



The total observed intensities and the optical appearances under static spherical accretion for the new regular BH with $n = 3$ and the corresponding Hayward BH.

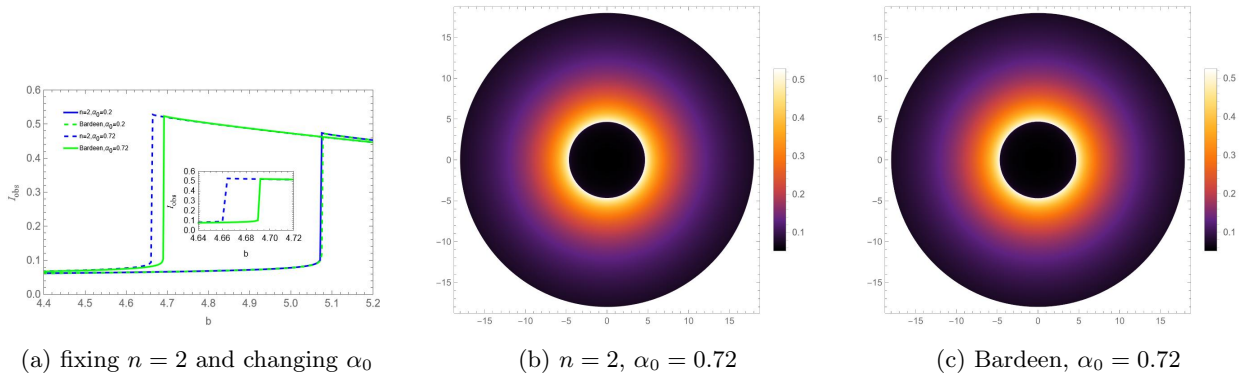
Secondly, Figs.(6b)(6c)(7b) and (7c) present the optical appearances of these BHs with different cores when $\alpha_0 = 0.72$ and $\alpha_0 = 0.92$ respectively. It can be clearly seen that the maximum luminosity of these regular BHs with a Minkowski core is significantly dimmer than that of the traditional regular BHs with a dS core. Moreover, the shadow and photon sphere radius of the former are also smaller than those of the latter. This indicates that, under the static spherical accretion model, compared with the traditional regular BHs, these new regular BHs have a weaker ability to capture photons, and the two exhibit different optical observational characteristics. Furthermore, as α_0 increases, the differences in optical observational characteristics between these regular BHs with different cores become more significant, making it easier to distinguish them from their optical features.

Finally, by comparing Figs.(6) and (7), it can be seen that under the static spherical accretion, the difference between the Bardeen BH and the new regular BH corresponding to $n = 2$ is more obvious than that between the Hayward BH and the new regular BH corresponding to $n = 3$. This once again proves that the smaller n is, the easier it is for observers to distinguish these regular

BHs with different cores.

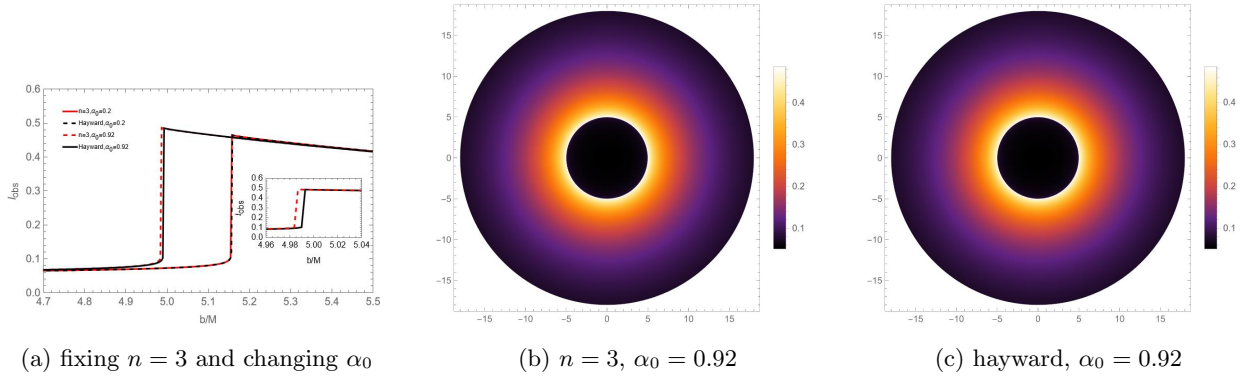
B. Comparison under the infalling spherical accretion

Under the infalling spherical accretion model, the total observed intensities and optical appearances of these new regular BHs with $n = 2$ and $n = 3$, and their corresponding Bardeen/Hayward BHs, are shown in Figs.8 and 9 respectively. It can be observed that, there are only slight differences in the shadows between the regular BHs with a Minkowski core and the traditional regular BHs with a dS core. As α_0 increases, the total observed intensity, shadow radius and photon sphere radius of the former are slightly smaller than those of the latter, and the maximum luminosity of the former is slightly dimmer than that of the latter. This difference becomes slightly more obvious only when α_0 is relatively large.



The total observed intensities and the optical appearances under the infalling spherical accretion for the new regular BH with $n = 2$ and the corresponding Bardeen BH.

The shadows of these new regular BHs with a Minkowski core and the corresponding traditional regular BHs with a dS core (Bardeen/Hayward BHs) are analyzed comparatively under two spherical accretion models. The shadows of these new regular BHs and the traditional regular BHs differ. Specifically, these new regular BHs have a smaller peak value of the total observed intensity, a dimmer maximum luminosity, as well as smaller shadow radius and photon sphere radius. Moreover, as α_0 increases, these differences become more pronounced, making it easier to distinguish these regular BHs with different cores through optical observational characteristics. In addition, these differences are more pronounced under the static spherical accretion model.



The total observed intensities and the optical appearances under the infalling spherical accretion for the new regular BH with $n = 3$ and the corresponding Hayward BH.

V. Conclusions

This paper explores the shadows of these new regular BHs with a Minkowski core under different spherical accretion models and compares them with the traditional regular BHs with a de Sitter (dS) core (Bardeen/Hayward BHs). The results reveal that in both the static sphere accretion and the infalling sphere accretion, the total observed intensity, shadow radius and photon sphere radius of these new regular BHs are closely associated with these intrinsic parameters. As the quantum gravity parameter α_0 increases, the total observed intensity, shadow radius, and photon sphere radius also increase. On the other hand, as the spacetime deformation parameter n increases, these values decrease. Moreover, the shadow radius and photon sphere radius are unaffected by the choice of the accretion model, while the total observed intensity differs between the models, with the higher total observed intensity in the static sphere accretion than in the infalling sphere accretion.

Secondly, there are difference in the shadows of the two types of regular BHs with different cores, and these differences are more obvious in static spherical accretion. Taking the new regular BH with a Minkowski core ($n = 2, x = 2/3$) and the Bardeen BH as an example, the former has a smaller total observed intensity, a dimmer maximum luminosity, smaller shadow radius and photon sphere radius, and a weaker ability to capture photons. More importantly, these differences become more significant as α_0 increases. Similarly, the new regular BH ($n = 3$ and $x = 1$) and the Hayward BH exhibit a similar trend. In the infalling sphere accretion, there are only subtle differences in total observed intensity, shadow radius, and photon sphere radius, and the differences are only

slightly more obvious when α_0 is relatively large.

In addition, the results show that the shadows can represent the intrinsic properties of the BH spacetime, and the choice of the accretion model only affects the total observed intensity of the shadows and does not affect the structure of the BH shadow itself. Therefore, the spacetime characteristics of these new regular BHs can be distinguished by observing and studying the BH shadow.

In this paper, we only apply two models: the static spherical accretion and the infalling spherical accretion. In fact, more complex accretion models can be studied, such as those incorporating the effects of magnetic fields or non-spherical accretion. It will help us to more comprehensively understand the changes in the shadows of BHs under different accretion scenarios and provide a more abundant theoretical foundation for astronomical observations. Meanwhile, we focus on the comparison of these new regular BHs with a Minkowski core and traditional regular BHs with a de Sitter core. In the subsequent research, the parameter range of the BHs can be expanded to study the shadows of BHs under more different parameter combinations. With the continuous progress of astronomical observation technology, the accuracy and breadth of observational data are constantly improving. The combination of theoretical research and actual observations should be strengthened. High resolution BH images and other observational data can be used to more accurately verify the theoretical models. By comparing the shadows calculated by theory with the actual observational results, the theoretical models can be continuously optimized to improve the understanding and knowledge of the properties of BHs. Furthermore, the correlations between the shadows of BHs and other astrophysical phenomena should be studied, such as the spin of BHs, the distribution and motion state of matter around BHs. Exploring how these factors jointly affect the observational characteristics of the shadow will contribute to more comprehensively understanding the physical processes around BHs and the role of BHs in galaxy evolution.

VI. Acknowledgements

This work is supported by Sichuan Science and Technology Program(2023NSFSC1352), and by the starting fund of China West Normal University (Nos. 20E069 and 20A013).

-
- [1] R. Abbott *et al.*, *LIGO Scientific Collaboration, Virgo Collaboration, and KAGRA Collaboration*, Phys. Rev. Lett. **118**, 221101 (2017); Phys. Rev. Lett. **851**, L35 (2017); Phys. Rev. Lett. **116**, 131103 (2018);

- Phys. Rev. Lett. **125**, 101102 (2020).
- [2] R. Abbott *et al.*, *LIGO Scientific and Virgo*, *Phys. Rev. D* **102** (2020), 043015.
- [3] R. Gold *et al.*, *Event Horizon Telescope Collaboration*, *Astrophys. J.* 897: 148 (2020).
- [4] J. C. McKinney, A. Tchekhovskoy, R. D. Blandford, *Mon. Not. R. Astron. Soc.* **423**, 3083 (2012).
- [5] K. Akiyama *et al.*, *Event Horizon Telescope Collaboration*, *Astrophys. J. Lett.* **930**, L12 (2022); *Astrophys. J. Lett.* **930**, L13 (2022); *Astrophys. J. Lett.* **930**, L14 (2022); *Astrophys. J. Lett.* **930**, L15 (2022); *Astrophys. J. Lett.* **930**, L16 (2022); *Astrophys. J. Lett.* **930**, L17 (2022).
- [6] J. M. Bardeen, Proceedings, École d'Été de Physique Théorique: Les Astres Occlus: Les Houches, France, August, 1972, 215–240 (1973).
- [7] J. M. Bardeen, W. H. Press, S. A. Teukolsky, *Astrophys. J.* **178**, 347 (1972).
- [8] N. I. Shakura, R. A. Sunyaev, *Astron. Astrophys.* **24**, 337-355 (1973).
- [9] J.-P. Luminet, *Astron. Astrophys.* **75**, 228-235 (1979).
- [10] S. E. Gralla, D. E. Holz, R. M. Wald, *Phys. Rev. D* **100**, 024018 (2019).
- [11] X. X. Zeng, H. Q. Zhang, H. Zhang, *et al.*, *Eur. Phys. J. C* **80**, 872 (2020).
- [12] X. X. Zeng, G. P. Li, K. J. He, *et al.*, *Nucl. Phys. B* **974**, 115639 (2022).
- [13] Y. Meng, X. M. Kuang, X. J. Wang, *Phys. Rev. D* **108**, 064013 (2023).
- [14] S. Guo, Y. X. Huang, Y. H. Cui, *et al.*, *Eur. Phys. J. C* **83**, 1059 (2023).
- [15] W. Zeng, Y. Ling, Q. Q. Jiang, *et al.*, *Phys. Rev. D* **108**, 104072 (2023).
- [16] K. J. He, S. Guo, S. C. Tan, *et al.*, *Chin. Phys. C* **46**, 085106 (2022).
- [17] Y. Meng, X. M. Kuang, X. J. Wang, *et al.*, *Phys. Rev. D* **108**, 064013 (2023).
- [18] X. X. Zeng, C. Y. Yang, Y. X. Huang, *et al.*, *arXiv:2501.13764 [gr-qc]*.
- [19] H. B. Zheng, M. Q. Wu, G. P. Li, *et al.*, *Eur. Phys. J. C* **85**, 46 (2025).
- [20] K. J. He, C. Y. Yang, X. X. Zeng, *et al.*, *arXiv:2501.06778 [astro-ph.HE]*.
- [21] H. B. Zheng, M. Q. Wu, G. P. Li, *et al.*, *Eur. Phys. J. C* **85**, 46 (2025).
- [22] S. Guo, G. R. Li, E. W. Liang, *et al.*, *Phys. Rev. D* **105**, 023024 (2022).
- [23] A. Urmanov, H. Chakrabarty, D. Malafarina, *Phys. Rev. D* **110**, 044030 (2024).
- [24] X. X. Zeng, K. J. He, G. P. Li, *et al.*, *Eur. Phys. J. C* **82**, 764 (2022).
- [25] G. P. Li, K. J. He, *JCAP* **06**, 037 (2021).
- [26] H. Rehman, G. Abbas, *Chin. Phys. C* **47**, 125106 (2023).
- [27] A. K. Ahmed, U. Camci, M. Jamil, *Class. Quant. Grav.* **33**, 215012 (2016).
- [28] M. Darvishi, M. Heydari-Fard, M. Mohseni, *Chin. J. Phys.* **93**, 632-648 (2025).
- [29] R. Kumar, S. G. Ghosh, *Astrophys. J.* **892**, 78 (2020).
- [30] J. Yang, C. Zhang, Y. Ma, *Eur. Phys. J. C* **83**, 619 (2023).
- [31] T. Johannsen, *Astrophys. J.* **777**, 170 (2013).
- [32] R. Takahashi, *J. Korean Phys. Soc.* **45**, S1808-S1812 (2004).
- [33] H. Falcke, F. Melia, E. Agol, *Astrophys. J. Lett.* **528**, L13 (2000).
- [34] J. Ovalle, R. Casadio, E. Contreras, *et al.*, *Phys. Dark Univ.* **31**, 100744 (2021).

- [35] E. Contreras, J. Ovalle, R. Casadio, *Phys. Rev. D* **103**, 044020 (2021).
- [36] C. Zhang, Y. Ma, J. Yang, *Phys. Rev. D* **108**, 104004 (2023).
- [37] X. X. Zeng, K. J. He, J. Pu, *Eur. Phys. J. C* **83**, 897 (2023).
- [38] J. Zhang, *Phys. Lett. B* **668**, 353-356 (2008).
- [39] R. Ali, X. Tiecheng, R. Babar, *Gen. Rel. Grav.* **56**, 13 (2024).
- [40] J. Zhang, *Phys. Lett. B* **675**, 14-17 (2009).
- [41] J. Yang, Y. Ma, *Chin. Phys. C* **43**, 103106 (2019).
- [42] E. Wilson-Ewing, *JCAP* **08**, 015 (2013).
- [43] B. Tan, *Phys. Lett. B* **861**, 139289 (2025).
- [44] R. Goswami, P. S. Joshi, P. Singh, *Phys. Rev. Lett.* **96**, 031302 (2006).
- [45] L. Xiang, Y. Ling, Y. G. Shen, *Int. J. Mod. Phys. D* **22**, 1342016 (2013).
- [46] S. B. Giddings, *Phys. Rev. D* **49**, 4078-4088 (1994).
- [47] C. A. Cabrera, D. Perini, T. A. Bampton, *et al.*, *IEEE Trans. Appl. Supercond.* **35**, 1-7 (2025).
- [48] R. Banerjee, B. R. Majhi, *Phys. Lett. B* **662**, 62-65 (2008).
- [49] A. Kaushal, N. S. Prabhakar, S. R. Wadia, [arXiv:2501.03926 [hep-th]].
- [50] S. Viaggiu, [arXiv:2501.04358 [hep-th]].
- [51] Y. Sekhmani, D. J. Gogoi, R. Myrzakulov, *et al.*, *Class. Quant. Grav.* **41**, 185002 (2024).
- [52] H. Singh, M. K. Nandy, *Gen. Rel. Grav.* **57**, 32 (2025).
- [53] A. del Rio, *Gen. Rel. Grav.* **57**, 30 (2025).
- [54] A. T. Taiba, A. Boudjemâa, *Phys. Lett. B* **861**, 139291 (2025).
- [55] S. Leutheusser, H. Liu, *Phys. Rev. D* **108**, 086019 (2023).
- [56] N. Kumar, *Phys. Lett. B* **861**, 139264 (2025).
- [57] S. Nojiri, S. D. Odintsov, *Phys. Dark Univ.* **46**, 101669 (2024).
- [58] Y. Ling, M. H. Wu, *Class. Quant. Grav.* **40**, 075009 (2023).
- [59] A. Simpson, M. Visser, *Universe* **6**, 8 (2019).
- [60] B. Yang, G. He, Y. Xie, *et al.*, *Eur. Phys. J. C*, **84**, 907 (2024).
- [61] M. Y. Guo, M. H. Wu, X. M. Kuang, *et al.*, *Eur. Phys. J. C* **85**, 95 (2025).
- [62] W. Zeng, Y. Ling, Q. Q. Jiang, *Chin. Phys. C* **47**, 085103 (2023).
- [63] D. P. Theodosopoulos, T. Karakasis, G. Koutsoumbas, *et al.*, *Eur. Phys. J. C* **84**, 592 (2024).
- [64] R. R. Cuzinatto, E. M. de Moraes, B. M. Pimentel, *Class. Quant. Grav.* **41**, 165007 (2024).
- [65] M. Yasir, F. Mushtaq, X. Tiecheng, *et al.*, *Phys. Dark Univ.* **48**, 101838 (2025).
- [66] M. Wang, G. Guo, S. Chen, *et al.*, *Chin. Phys. C* **47**, 015102 (2023).
- [67] M. Wang, G. Guo, P. Yan, *et al.*, *Chin. Phys. C* **48**, 105103 (2024).
- [68] F. Atamurotov, I. Hussain, G. Mustafa, *et al.*, *Chin. Phys. C* **47**, 025102 (2023).
- [69] Y. Z. Du, H. F. Li, X. N. Zhou, *et al.*, *Chin. Phys. C* **46**, 122002 (2022).
- [70] S. Nalui, S. Bhattacharya, *Phys. Lett. B* **861**, 139261 (2025).
- [71] S. Giri, U. Danielsson, L. Lehner, *et al.*, *Phys. Rev. D* **111**, 024007 (2025).

- [72] H. L. Li, M. Zhang, Y. M. Huang, *Eur. Phys. J. C* **84**, 860 (2024).
- [73] Y. Heydarzade, M. Misyura, V. Vertogradov, *Phys. Rev. D* **108**, 044073 (2023).
- [74] N. U. Molla, H. Chaudhary, S. Capozziello, *et al.*, *Phys. Dark Univ.* **47**, 101804 (2025).
- [75] Jin Pu, Qin-Bin Mao, Qing-Quan Jiang, *et al.*, *Chin. Phys. C* **44**, 095103 (2020).
- [76] A. Das, S. Das, E. C. Vagenas, *Phys. Lett. B* **809**, 135772 (2020).
- [77] S. Nojiri, S. D. Odintsov, *Phys. Dark Univ.* **46**, 101669 (2024).
- [78] G. Bhandari, S. D. Pathak, M. Sharma, *et al.*, *Gen. Rel. Grav.* **56**, 139 (2024)
- [79] S. Das, E. C. Vagenas, *Phys. Rev. Lett.* **101**, 221301 (2008).
- [80] H. Cheng, Y. Zhong, *Chin. Phys. C* **45**, 105102 (2021).
- [81] H. Bondi, *Mon. Not. Roy. Astron. Soc.* **112**, 195 (1952).
- [82] S. M. Ressler, L. Combi, B. Ripperda and E. R. Most, *Astrophys. J. Lett.* **979**, L24 (2025).
- [83] F. Yuan, R. Narayan, *Ann. Rev. Astron. Astrophys.* **52**, 529-588 (2014).
- [84] M. Jaroszynski, A. Kurpiewski, *Astron. Astrophys.* **326**, 419 (1997).
- [85] N. Roy, *Mon. Not. Roy. Astron. Soc.* **378**, L34-L38 (2007).
- [86] C. Bambi, *Phys. Rev. D* **87**, 107501 (2013).